EUV Actinic Imaging Tool Aerial Image Evaluation of EUVL Embedded Phase Shift Mask Performance

Pei-Yang Yan[1], Iacopo Mochi[2], and Ken Goldberg[2]
[1]Intel Corporation, 3065 Bowers Ave. Santa Clara, CA 95092
[2]Lawrence Berkeley National Laboratory, 1 Cyclotron Rd., Berkeley, CA 94720

ABSTRACT

Extreme Ultraviolet Lithography (EUVL) embedded phase shift mask (EPSM) can further extend lithography resolution limit and provide better pattern fidelity as compared to that of EUVL binary mask for 16nm node technology and beyond generations. In our previous study, we have demonstrated in wafer printing that EUVL EPSM can provide improved process window for both the dense lines and contacts and the low shadowing effect when compared to that of the EUVL binary mask. Due to limitation of current EUVL resist performances, certain advantages of EUVL EPSM, such as line width roughness (LWR) improvement, cannot be readily seen at wafer resist level. This is because that the aerial image quality improvement in LWR is over shadowed by the current large resist intrinsic and process induced LER. We believe that when EUV resist and wafer process improves in future, mask induced pattern fidelity difference will start to play an observable role in wafer printing. In this study, we focused on comparing EUV actinic aerial image performance of a EUVL EPSM and a binary mask for both lines and contacts. Without convoluting with resist effect, the mask aerial image performance comparison of two different masks can better reflect all the effects that are due to mask differences. Our analysis of the EUV actinic aerial images of a EUVL EPSM and a binary mask showed not only the process window advantages of the EPSM as demonstrated previously, but also the improved LWR performance of EUVL EPSM when compared to that of the EUVL binary mask. The matrix used to analyze the aerial images includes aerial image contrast, LWR, process windows (focus-exposure plot), etc. Our detailed analysis is performed for various line and contact features.

Key words: Extreme ultraviolet lithography, Embedded phase shift mask, Phase error, EUVL absorber, Extreme ultraviolet lithography mask, Multilayer mask blanks.

1. INTRODUCTION

Phase shift mask has been widely used in the semiconductor lithography process to enhance the pattern contrast. Among the different types of phase shift masks, the attenuated phase shift mask which combines the attenuation and 180-degree phase shift in the mask absorber region is a simple one to adopt. When the selected mask absorber material satisfies both the light attenuation and phase requirement, such material is also referred to as embedded phase shift material and the corresponding attenuated phase shift mask is referred to as embedded phase shift mask (EPSM). Although EPSM is a weak phase shift mask which provides only limited imaging improvement, it is attractive due to its simplicity in fabrication (similar to that of the conventional mask fabrication). EUVL EPSM application and performance have been previously studied by several authors.[1-5] Last year, we have conducted detailed wafer level study of a 6% EUVL EPSM and EUVL binary mask via ADT wafer exposure.[6-7] In the experiment, we used SEVR59 resist and the exposure conditions of numeric aperture (NA) NA=0.25, partial coherence σ=0.5. Our results showed that EUVL EPSM has advantages in many aspects of wafer printing as compared to that of the EUVL binary mask. These advantages include a larger process window and better resolution for dense lines and contacts, a smaller shadowing effect, and a lower dose-to-target. In this study, we used the same two masks for imaging under the Berkeley National Lab's EUV actinic inspection tool (AIT) for dense lines and contacts. The aerial image analysis was performed to extrapolate the image contrast, line width roughness, and focus-exposure latitude to understand the performance difference between the two masks. Since no resist is involved, the aerial image difference between the two types of mask can be easily compared. In addition, the 0.35 NA of the AIT used for the aerial image collection will further allow us to access the performance of both EUVL EPSM and binary mask at high NA as compared to that in the ADT. We expected to see better resolution limit for the two masks as compared to that of our earlier obtained lower NA ADT wafer printing results.

Extreme Ultraviolet (EUV) Lithography III, edited by Patrick P. Naulleau, Obert R. Wood II, Proc. of SPIE Vol. 8322, 83221P · © 2012 SPIE
CCC code: 0277-786X/12/$18 · doi: 10.1117/12.919710

In this study, we have evaluated and compared EUVL EPSM and binary mask imaging performance for small dense lines at 18nm under the conventional illumination and the equivalent off-axis illumination in terms of resolution and LWR performance; lager line feature aerial image resolution and LWR under the conventional illumination, and contacts process latitude (focus-exposure latitude) under the conventional illumination. In section 2, the detailed mask information is given. In section 3, the EUVL actinic images of the mask features and the corresponding image analysis results will be presented. The performance difference of the two masks will also be discussed. Section 4 is the conclusion.

2. EUVL EPSM AND BINARY MASK INFORMATION

In our experiment, the EUVL EPSM and the binary mask were fabricated at the same time for the performance comparison purposes. Both EUVL EPSM and binary mask fabrication used EUVL ML blank with low thermal expansion material (LTEM) substrates. The EUVL ML blank contains 50 bi-layers of molybdenum and silicon (Mo/Si) and a 2.5nm Ru capping layer. The EPSM mask absorber stack used TiN/TaN two-film combination. Although there are other material candidates for EUVL EPSM, the selection of TiN/TaN combination has also been taking into account the availability of the current mask fabrication process steps. In Fig. 1, a schematic drawing of the EUVL EPSM and binary mask is given.

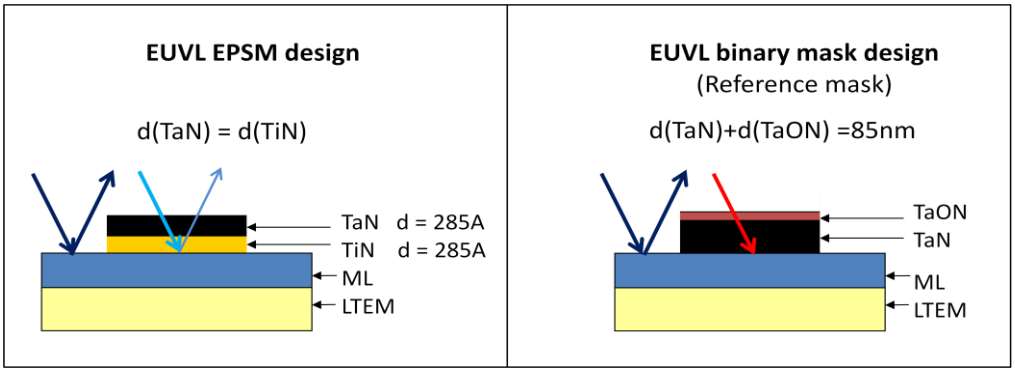

Fig. 1 Schematic draw of EUVL EPSM and EUVL binary mask design. The EUVL EPSM absorber material is a TiN/TaN bi-layer with thickness of 285A each.

In EUVL EPSM fabrication, we targeted the normalized EUV reflection in the EPSM absorber region at 6% (with ML reflectivity normalized to 100%). Based on the EPSM absorber film optical constant n and k values, the film thickness required for EUVL EPSM at 13.5nm is $d_{TiN} \approx d_{TaN} \approx 28.5$nm. The corresponding absorber leakage relative to the ML reflectivity (normalized to 100%) is about 6%. The EUVL binary mask consists of the standard TaN/TaON film stack, where TaON serves as an anti-reflection layer for DUV (248nm) wavelength to enhance the patterned mask inspection contrast.[8-9] The combined TaN/TaON film thickness is about 85nm. The EUV light leakage measured in the TaN/TaON absorber region is <0.5% which is the typical leakage value for the standard EUVL binary mask. Both the patterned EUVL EPSM and the binary mask have ~ 63% EUV reflectivity at 13.5nm in the ML region. For the comparison purposes, the EUVL binary mask is also referred as the reference mask when compared to the EPSM in later sections. In table 1, the measured EUV reflectivity at the ML region for both the patterned EUVL EPSM and binary mask is given. It is shown that the EUV reflectivity characteristics of the two masks in the ML region are very similar. In Fig. 2 the plot of the EUV reflectivity spectrum of the EUVL EPSM in the absorber region is given. As expected, the normalized EUV reflectivity (ML reflectivity = 1) at 13.5nm in the EPSM absorber region is about 6%.

	R (%)	Centroid λ (nm)
EPSM	63.17	13.497
Binary	63.18	13.560

Table 1 EUV reflectivity of the EUVL EPSM and binary mask in the ML region.

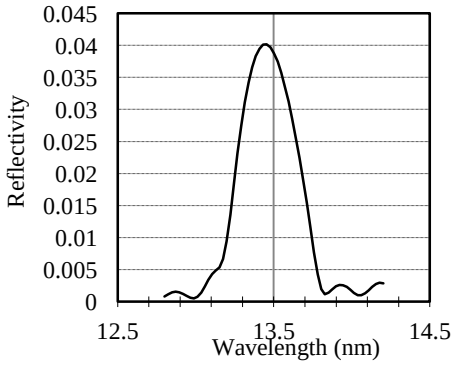

Fig. 2 EPSM EUV reflectivity spectrum in the absorber region.

3. AIT IMAGING RESULTS AND DISCUSSIONS

EUV actinic inspection tool is a zone plate microscope using synchrotron beam as an illumination source.[10] The AIT has adjustable NA and magnification. The NA value used in our experiment is 0.35 which emulates the next generation EUVL printing tool. The partial coherence is estimated between 0.15 and 0.2.

3.1 Dense Line Performance

Since AIT provides higher NA than the currently available EUV exposure tool, we are interested in explore the resolution limit of the two masks and compare their performance. We evaluated the images taken at both the AIT CCD center and the off-center locations which is a perpendicular distance from the center vertical lines. The images at the off-center location have an off-axis illumination effect. As a result, we are expecting an improved resolution and depth of focus (DOF) due to off-axis illumination for the dense lines. Although the imaging lens (zone plate) has larger aberration at the off-center locations, these aberrations have less impact for the vertical lines. In Fig. 3, a typical AIT low magnification image of the 18nm dense vertical lines is given. The left circle location is the image center location and the right circle location is the image off-center location that used in our data analysis. This off-center image location used in the experiment is about 70 feature-periods from the center image. The pattern in Fig. 3 is the 18nm L/S (1x), therefore, the distance from the image center (4x) is 36nm x 4 x 70 = 10.08mm. This off-axis location is used for evaluation of both EUVL EPSM and binary mask.

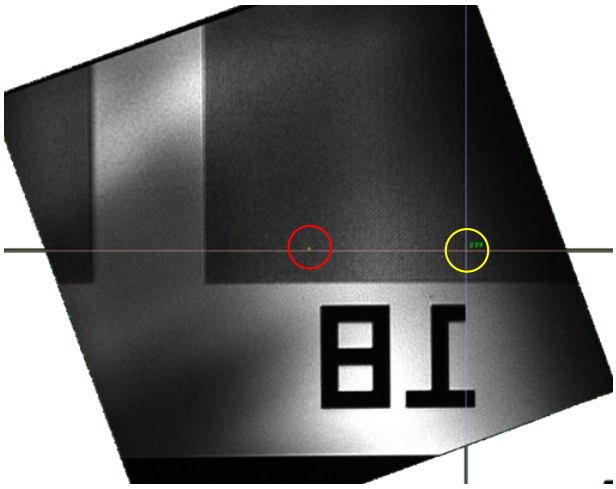

Fig. 3 AIT images of 18nm L/S. The circle locations in the left and right are the center and off-center image locations used in our analysis, respectively.

To explore the mask performance at the resolution limit, we collected the aerial images of the dense lines through focus for both masks. For quantitative aerial image analysis and comparison, in additional to the direct aerial image comparison, we used aerial image contrast and aerial image LWR as the additional comparison matrices. The feature sizes selected for the study are the dense lines of 18nm, 19nm, and 34nm, respectively. The off-center aerial image analysis is also performed for 18nm L/S. In Fig 4, the comparison of center aerial images through focus for both EUVL EPSM and binary masks are given. It is showed that the EUVL binary mask aerial images had very little contrast or intensity modulation at this feature size. The EPSM showed higher image contrast than that of the binary mask. To further quantify the image contrast, we analyzed the aerial image intensity given in Fig.4 through focus. The aerial image contrast defined as (Imax-Imin)/(Imax+Imin) was extrapolated from the aerial image intensity analysis. In Fig. 5, the plot of aerial image contrast of the two masks as a function of defocus is given. It is shown that the EUVL binary mask's aerial image contrast is only about 23% at the best focus. This contrast is too low to print any resist line, indicating the

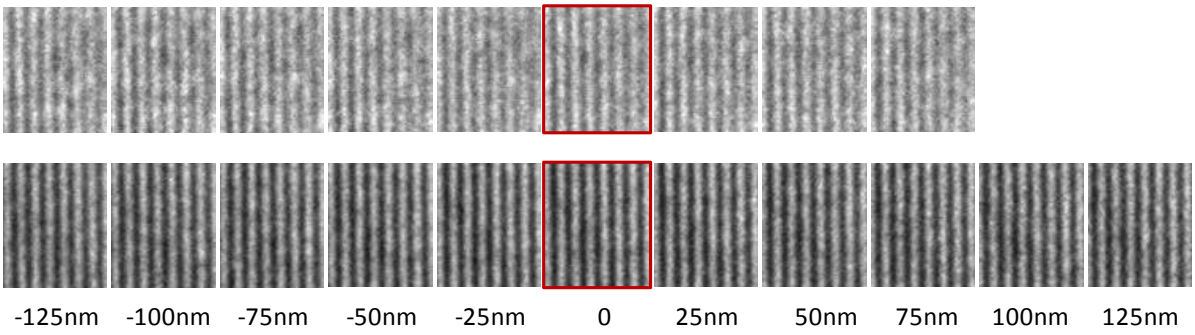

Fig. 4 AIT center images of 18nm L/S through focus. The top row is the aerial images obtained from EUVL binary mask. The bottom row is that from EUVL EPSM. The defocus values are given in the wafer plane.

imaging resolution limit at this feature for this mask. For NA of 0.35, printing 18nm half- pitch lines corresponds to a k1 factor of 0.47. When no image enhancement techniques, such as phase shift mask, off-axis illumination, etc., applied, it will be indeed difficult to achieve high image contrast with this low k1 value. The aerial image contrast for the EUVL EPSM at this small feature is about 50% which is much better than that of the EUVL binary mask although it is still marginal to printing the resist lines.

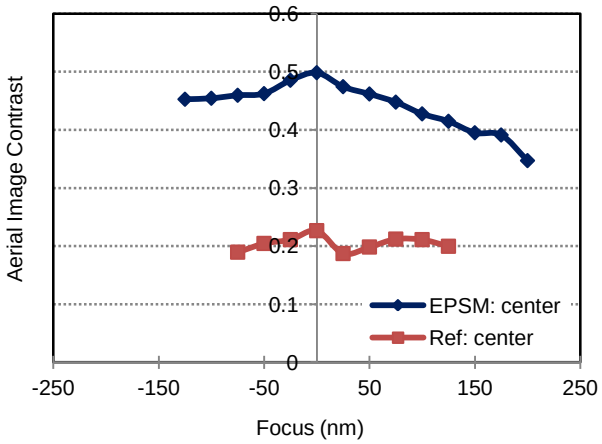

Fig. 5 AIT aerial image contrast of 18nm L/S of the EPSM and binary mask collected at the image center location. The defocus values are given in the wafer (1x) plane.

To extend the mask resolution limit for a given NA, one of the enhancement techniques is to using the off-axis illumination. In our experiment use AIT imaging the mask, the off-axis illumination image can be obtained by using the aerial images that are at the off-center location as indicated in location by the right circle in Fig. 3. Although the AIT provides the minimum aberration at image center, we found that the aberration impact to the off-center image has less of effect for the vertical lines as compared to that of the contacts. As a result, we are able to obtain good aerial image quality for the vertical lines located off-center. In Figs. 6 and 7, the aerial image contrast and LWR comparison between the EUVL EPSM and binary mask for 18nm L/S at the off-center (equivalent of off-axis illumination) location are given. It is shown from Fig. 6 that the aerial image contrast for both masks has drastically improved. The EUVL binary mask aerial image contrast increased from 23% to 56% and the EUVL EPSM aerial image contrast increased from 50% to 65% at the best focus, respectively. The aerial image contrast of EUVL EPSM is continuously higher than that of EUVL binary mask at the off-axis illumination condition. Further examining the line width roughness via aerial image analysis of the two masks, we found that EPSM is again superior to the binary mask. This is not surprising as higher contrast aerial images typically will result in a better pattern fidelity.

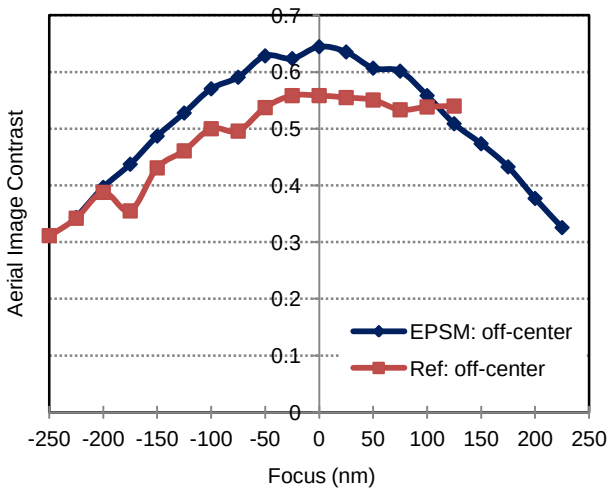

Fig. 6 AIT aerial image contrast of 18nm L/S of the EPSM and binary mask collected at the image off-center location as a function of defocus. The image obtained at the off-center location is similar to that obtained under the off-axis illumination. As a result, the image contrast is greatly improved. The defocus values are given in the wafer (1x) plane.

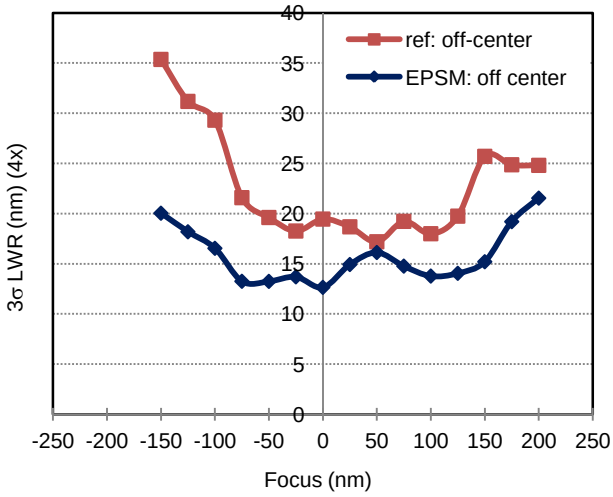

Fig. 7 LWR of 18nm L/S of the EPSM and binary mask as a function of defocus. The LWR is extrapolated from AIT aerial image at the off-center location. The defocus values are given in the wafer (1x) plane.

In Fig. 8, the AIT aerial images of 18nm L/S at the off-center location for the two masks are given. The top row is the binary mask aerial images and the bottom row is the EPSM aerial images. The aerial images for both masks are

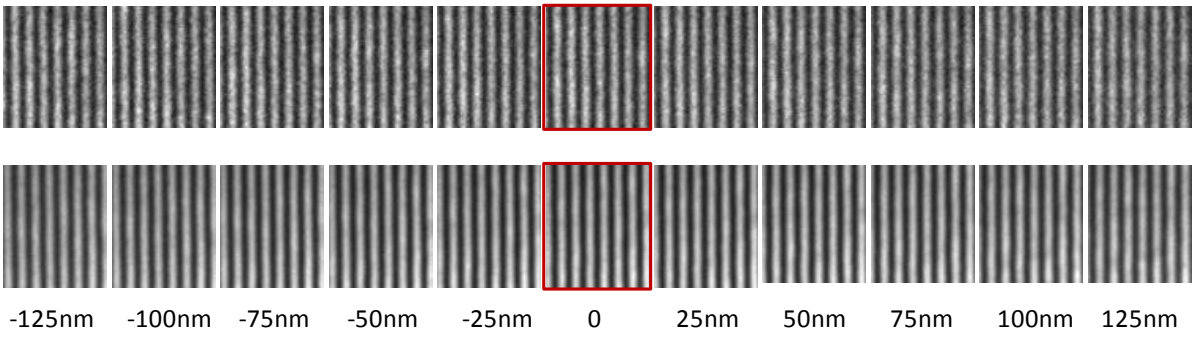

Fig. 8 AIT off-center images of 18m L/S through focus. The top row is the aerial images obtained from EUVL binary mask. The bottom row is that from EUVL EPSM. The focus values are given in the wafer plane.

evaluated at the same image off-center location. It is clearly shown the improvement of the aerial image contrast and depth-of-focus (DOF) for both masks when compared to that in the image center location. The EUVL EPSM images showed a better performance than that of the reference mask. By carefully compare the line edge of the two rows, it is also shown that the EPSM aerial images have a smoother line edge than that of the binary mask. This is consistent with the LWR difference obtained through aerial image intensity analysis.

To quantify the amount of aerial image performance between the two masks, we further compared the center aerial images through focus for the two masks at 19nm L/S. In Fig. 9, the plot of the aerial images through focus for the two masks is given. The top row is the binary mask images and the bottom row is the EPSM images. It is shown from Fig. 9 that the aerial image contrast improved greatly for the binary mask when compare to that of 18nm L/S shown in Fig. 4. In fact, the aerial image analysis showed a contrast value of 51% for the binary mask at 19nm L/S. The aerial image contrast for the EPSM has also improved from 50% to 58%. Comparing the aerial image contrast of the binary mask at feature size of 19nm to that of the EPSM at feature size of 18nm (Fig. 5), we found that the two aerial image contrasts are about the same. It indicated that EPSM minimum resolution is about 1nm smaller than that of the binary mask. Since 6% EPSM is considered as weak phase shift mask, only small improvement over the binary mask is expected.

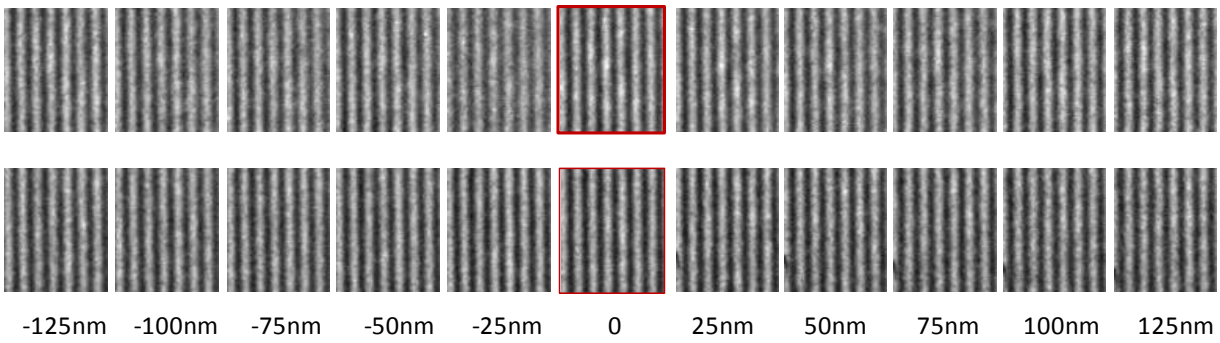

Fig. 9 AIT center images of 19nm L/S through focus. The top row is the aerial images obtained from EUVL binary mask. The bottom row is that from EUVL EPSM. The focus values are given in the wafer plane.

As we have indicated above that the poorer LWR performance of the binary mask at the resolution limit is obvious due to low aerial image contrast. The aerial image contrast difference between the two masks is also obvious at the mask resolution limit. However, at larger features, we would expect the aerial image performance to be similar for the two masks. Then the question is whether the LWR performance of the two masks is also the same? In Fig. 10, we have plotted the aerial image contrast evaluated at the image center as a function of defocus for 34nm L/S. It showed that both masks have high aerial image contrast around 90% at the best focus. The contrast defocus behavior of the two masks is also very similar. This is again no surprise as the advantage of the EPSM is for the small feature printing. We further

analyzed the LWR of the two masks for the same 34nm L/S feature and the results are given in Fig. 11. It is shown in Fig. 11 that EPSM is still slightly superior to the binary mask in LWR performance. The difference, however, is much smaller (about 0.75nm in 1x scale) as compared to that of 18nm L/S.

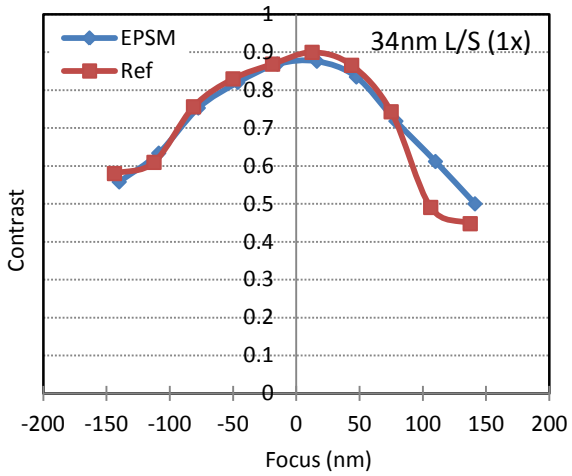

Fig. 10 AIT aerial image contrast of 34nm L/S of the EPSM and binary mask collected at the image off-center location. The defocus values are given in the wafer (1x) plane.

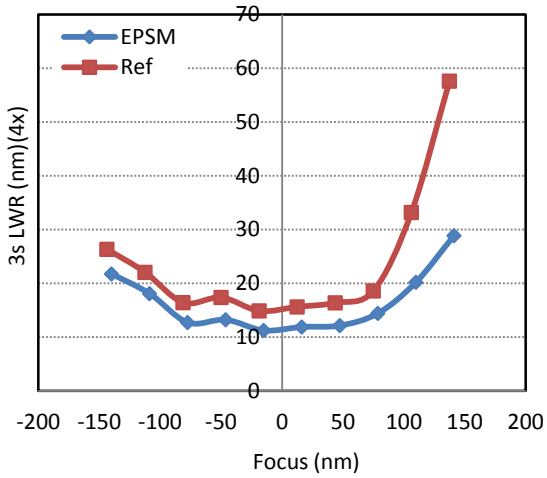

Fig. 11 LWR of 34nm L/S of the EPSM and binary mask as a function of defocus. The LWR is extrapolated from AIT aerial image at off-center location. The defocus values are given in the wafer (1x) plane.

3.2. Dense Contact Performance

For the contact performance evaluation, we collected AIT aerial images of the contrast at different sizes. The aerial image analysis of these images is focused on the process window or focus-exposure latitude performance. For contrast resolution assessment, we analyzed 28nm dense contacts of the two masks. First, we compared the aerial image appearance of the two masks through focus side by side as shown in Fig. 12. The aerial images on the top row are from

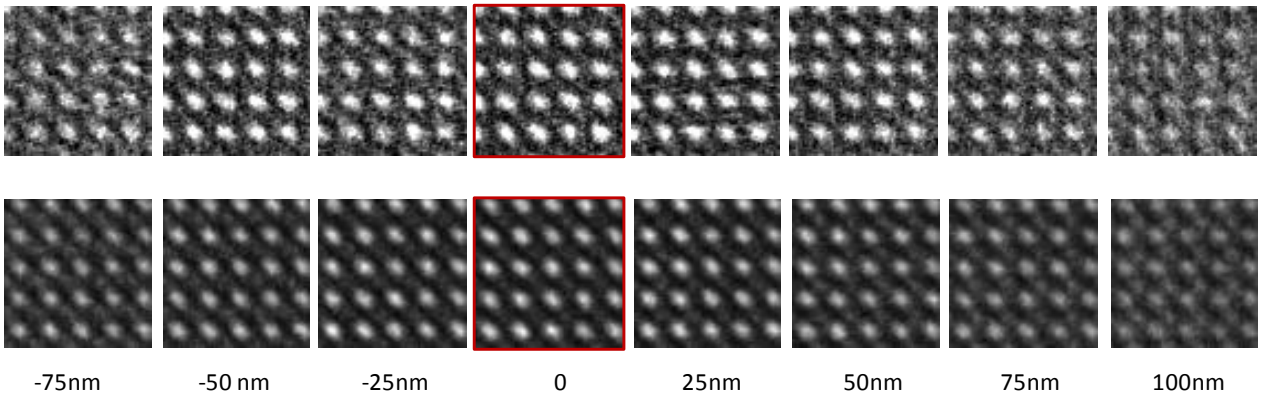

Fig. 12 AIT center images of 28nm dense contacts through focus. The top row is the aerial images obtained from EUVL binary mask. The bottom row is that from EUVL EPSM. The focus values are given in the wafer plane.

the binary mask and that on the bottom row are from EPSM. It appeared that EUVL EPSM has larger focus latitude than that of the binary mask by comparing the last defocus images on each side of the two masks. It is also worth to mention that the side lope started to appear for EPSM at larger defocused condition (e.g., at 100nm defocused condition, small side lope clearly showed up between the contact. However, this small side lope may not be printable in wafer printing).

To further perform a quantitative process window comparison, we extrapolated the focus-exposure latitude from the aerial images. For the process window analysis, a target CD and an allowable CD range needs to be specified. In our data analysis for the above 28nm dense contacts, the target CD of 28nm and the allowed CD range of ± 2.8nm (10% CD) are applied. The plot of 28nm dense contacts exposure latitude vs. focus latitude for an allowable 10% CD variation is given in Fig. 13. It is shown in Fig. 13, for any given percentage exposure latitude, EPSM has consistent larger DOF than that of the binary mask.

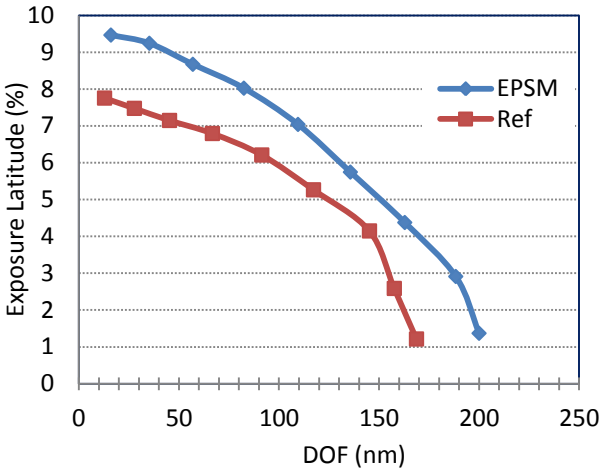

Fig. 13 F-E latitude of 28nm contacts of the EPSM and binary mask. The defocus values are given in the wafer (1x) plane.

Similar to that of the dense line case, we see an obvious process window improvement of the EUVL EPSM as compared to that of the binary mask at small contact features near the resolution limit. For larger contact feature sizes, the amount of improvement by EPSM can be limited as shown in Figs. 10-11 for the dense line case. To understand the performance difference between the two masks at larger contact size, we collected AIT aerial images of the 36nm dense contacts. The aerial images of the contact from the two masks are given in Fig. 14. The top row is the aerial images of the EUVL binary mask and the bottom row is that of EPSM. Please note that the images collected for the EPSM and binary mask are at different focus steps. By comparing the two rows of images, we found that the process window of the two masks for 36nm dense contacts is similar (e.g., comparing the two images at 125nm defocus position). This result is consistent with the case of dense lines, i.e., more improvement via EPSM can be obtained at the smaller features and the similar performance for the larger features.

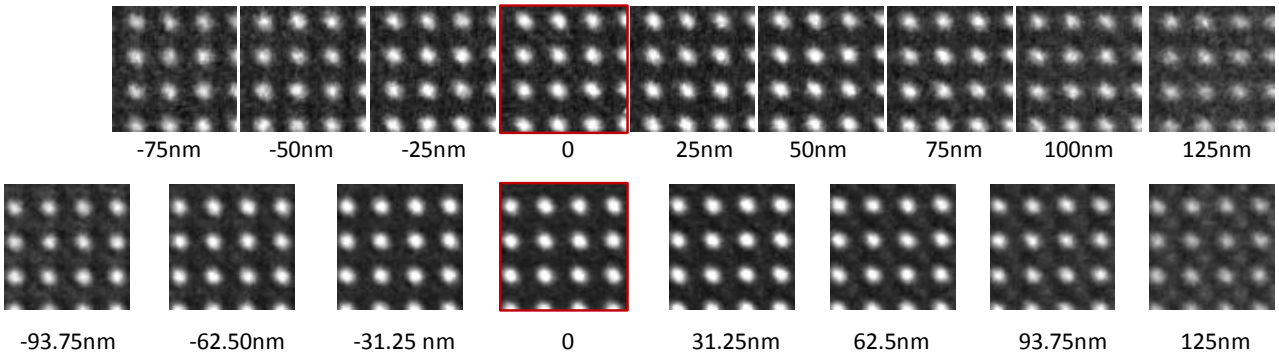

Fig. 14 AIT center images of 36nm dense contacts through focus. The top row is the aerial images obtained from EUVL binary mask. The bottom row is that from EUVL EPSM. Please note that the defocus step used it the top row and the bottom row are not the same. The focus values are given in wafer plane.

4. CONCLUSIONS

In this study, we have analyzed EUV AIT images of 18nm, 19nm, and 34nm dense lines and 28nm and 36nm contacts for both the EUVL EPSM and the binary mask using NA of 0.35. The aerial image intensity analysis is performed to obtain the aerial image contrast and LWR for dense lines and process window for the contacts. The off-center aerial image which is equivalent to that of under the off-axis illumination is also analyzed for 18nm L/S. The comparison of the analysis results between the EUVL EPSM and binary mask showed that EUVL EPSM has about 1nm resolution advantage than that of the binary mask. Under the conventional illumination (on-axis illumination), the dense

line resolution limit for the EUVL EPSM is about 18nm and for the binary mask is bout 19nm. The off-axis illumination can further improve the resolution and process window (e.g., exposure and focus latitude) for both masks. Therefore, combining the off-axis illumination and EUVL EPSM can further extend resolution limit defined by EUVL EPSM under the conventional on-axis illumination. The EUVL EPSM also showed much better LWR performance than that of the binary mask at small features due to better aerial image quality. At larger line features, the aerial image contrast of the two masks become similar. In the case of contacts, the aerial image analysis showed that for any given exposure latitude, EUVL EPSM consistently having larger DOF than that of the binary mask. At larger contact features, the performance difference starts to diminish. Therefore, the advantage of the EPSM is mainly to improve the binary mask performance at smaller features of both dense lines and contacts.

ACKNOWLEDGEMENT

The authors would like to thank Vijayakumar Ramachandrarao, Armando Cobarrubia, and Robert Chen for support of mask fabrication.

REFERENCES

1. S-I. Han, J. R. Wasson, P. J. S. Mangat, J. L. Cobb, K. Lucas, and S. D. Hector, “Novel Design of Att-PSM Structure for Extreme Ultra Violet Lithography and Enhancement of Image Contrast During Inspection.” Proc. SPIE 5037, 314 (2003).
2. M. Sugawara, A. Chiba and I. Nishiyama, “Design of Phase-Shift Masks in Extreme Ultraviolet Lithography.” Jpn. J. Appl. Phys. 42, 2639 (2003).
3. M. Sugawara, A. Chiba, H. Yamanashi, H. Oizumi and I. Nishiyama, “Attenuated Phase-shift Mask for Line Patterns in EUV Lithography,” Microelectronic Engineering 67-68, 10-16 (2003).
4. S-I. Han, E. Weisbrod, J. R. Wasson, R. Gregory, Q. Xie, P. J. S. Mangat, S. D. Hector, W. J. Dauksher, and K. M. Rosfjord, “Development of Phase Masks for Extreme Ultra Violet Lithography and Optical Evaluation of Phase Shift Materials.” Proc. SPIE 5374, 261 (2004).
5. H. Y. Jung, Y. R. Park, Y. R.; H. J. Lee, N-E. Lee, C. Y. Jeong, J. Ahn, "Selective Dry Etching of Attenuated Phase-shift Mask Materials for Extreme Ultraviolet Lithography Using Inductively Coupled Plasmas," J. of Vac Sci & Tech B 27 (6), 2361 (2009).
6. P. Y. Yan, M. Leeson, S. Lee, G. Zhang, E. Gullikson and F. Salmassi, "Extreme Ultraviolet–embedded Phase-shift Mask", J. Micro/Nanolith. MEMS MOEMS 10, 033011 (2011).
7. J. V. Hermans, E. Hendrickx, D. Laidler, C. Jehoul, D. V. D. Heuvel and A. Goethals, "Performance of the ASML EUV Alpha Demo Tool", Proc. SPIE 7636, 76361L (2010).
8. T. Liang, A. Stivers, P. Y. Yan, E. Tejnil and G. Zhang, “Enhanced Optical Inspectability of Patterned EUVL Mask,” Proc. SPIE 4562, 288-96 (2002).
9. D. Pettibone, A. Veldman, T. Liang, A. Stivers, P. Mangat, B. Lu, S. Hector, J. Wasson, K. Blaedel, E. Fisch, D. M. Walker, “Inspection of EUV Reticles” Proc. SPIE 4688, 363 (2002).
10. K. Goldberg, P. Naulleau, A. Barty, S. Rekawa, C. Kemp, R. Gunion, F. Salmassi, E. Gullikson, E. Anderson, and H. Han, “Performance of Actinic EUVL Mask Imaging Using a Zoneplate Microscope,” Proc. SPIE 6730, 67305E (2007).